PHYSICAL REVIEW B VOLUME 24, NUMBER 6 15 SEPTEMBER 1981

Ballistic phonons and the shape of the ray surface in cubic crystals

A. G. Every
Department of Physics, University of the Witwatersrand, Johannesburg 2001, South Africa
(Received 11 March 1981)

The shape of the acoustic ray surface of cubic crystals is investigated with the object of providing a framework within which the results of phonon imaging and other ballistic phonon experiments can be interpreted. This surface is shown to display considerable variability in shape, particularly with regard to the way in which it is folded. The correspondence between these folds and contours of zero Gaussian curvature on the slowness surface is explored, and the bearing this has on the presence of caustics in the anistropic flux of phonons emanating from a localized hear source is discussed. Several of the elementary catastrophes as well as some remarkable types of structural instability are shown to occur in these caustics. Conditions on the elastic constants are established for the existence of various systems of folds in the ray surface.

I. INTRODUCTION

The velocity, slowness, and ray surfaces are invaluable aids to the understanding of the nature of acoustic-wave propagation in elastically anisotropic solids. Indeed, it is difficult to imagine how the subject of crystal acoustics could be developed without these constructs. The ray surface is physically the most meaningful of the three in that it represents the wave front or surface of equal phase for an oscillatory disturbance a unit time interval after it has been created at the origin. It also happens to be the most complicated of the three. In spite of its importance, our knowledge of the ray surface is very limited. While the analytical techniques for generating this surface are well established, only a relatively small number of substances have been investigated by these means.[1,2] There have been several papers of a general nature in this area, but they have tended to emphasize issues such as conditions for the existence of cuspidal edges in symmetry planes,[3-6] and phonon-enhancement factors in specific directions,[6-8] and have not provided much information on the overall shape of the ray surface.

The status of this problem has been considerably enhanced by the recent surge of interest in phonon imaging,[9-12] a technique that employs ballistic phonons to probe the effects of elastic anisotropy and surface scattering on phonon transport. This knowledge is of particular importance for the understanding of low-temperature thermal conductivity,[13] Kapitza resistance,[14] and the shape of electron-hole droplet clouds in semiconductors.[15] Imaging experiments have yielded complex phonon-intensity maps which show numerous sharp features where the phonon flux is much higher than in the background. These sharp features represent caustics[10,11] and are associated with folding edges in the ray surface. With the high-resolution time of flight techniques that are now available for the study of ballistic phonons,[16] one can anticipate a rapid increase in the generation of detailed experimental data on the ray surface and related matters.

The above considerations have motivated the theoretical investigation which we report in this paper. A systematic survey has been carried out to determine all the topologically distinct shapes that the ray surface of cubic crystals can take on under the conditions that the elastic constants satisfy the thermodynamic constraints and the longitudinal phase velocity is greater than the two transverse velocities in all directions. It is hoped that this study will assist investigators in interpreting their experimental results and also provide some guidance for the selection of specimens and the design of experiments.

The slowness surface, which is the polar reciprocal of the ray surface, plays an important role in the discussion. It is a much simpler surface to which one can trace, and thereby gain a deeper appreciation of, all the important features of the ray surface. Catastrophe theory provides a ready framework for the description of the folding edges of the ray surface and the associated caustics in the phonon intensity.[14] For the most part these caustics can be categorized as one or other of the elementary catastrophes, but a number of remarkable cases of structural instability also occur.

The method that is used for the actual construction of the ray surface consists of calculating a set of points representing the group-velocity vectors for a large number of waves with normals distributed uniformly over the unit sphere. The distribution of these points corresponds, to within a factor $\sim 1/v^3$ to the distribution of thermal energy in a system a unit time interval after a pulse of heat has been injected at the origin. In this way one obtains a representation of the ray surface as well as a phonon-enhancement map for ballistically propagating heat pulses.

Section II of this paper deals with the theoretical background and the methods used in the computations. Restrictions on the elastic constants, which are used to limit the range of the survey, are discussed.

In Sec. III the effect that elastic anisotropy has on the three sheets of the slowness and ray surfaces is described. The emphasis is placed on determining what folds the ray surface has, and what the associated effects are.

II. BACKGROUND THEORY

A plane acoustic bulk wave in an elastically anisotropic medium is governed by the Christoffel characteristic equation[17]

$$|\Gamma_{rs} - \rho v^2 \delta_{rs}| = 0, \tag{1}$$

where v is the phase velocity of the wave, ρ is the density of the medium, and Γ_{rs} is the Christoffel tensor which, in the case of cubic symmetry, is given in terms of the elastic constants C_{ij} and components of the wave normal $\vec{n} = (n_i)$ by

$$\Gamma_{rs} = \begin{cases} (C_{12}+C_{44})n_r n_s & (r \neq s) \\ C_{11}n_r^2 + C_{44}(n^2 - n_r^2) & (r = s). \end{cases} \tag{2}$$

Expanding the determinant in Eq. (1) results in a cubic equation in v^2 which yields three values of the velocity for each direction $\vec{n}$. A convenient method of solving this cubic, which leads to closed-form expressions for the velocities, has been developed by this author.[18] The function $v(\vec{n})$, which is homogeneous of degree 1 in the components of $\vec{n}$, defines a centrosymmetric surface of three sheets known as the velocity or normal surface. The equation for this surface is of degree 12 in v as may easily be verified by multiplying Eq. (1) by v^6. As regards cubic symmetry, the three sheets remain separated except along the fourfold $\langle 100 \rangle$ axes where the transverse sheets make smooth contact, and along the threefold $\langle 111 \rangle$ axes where the transverse sheets meet at a conical point.[19]

The slowness surface is the inverse of the velocity surface and represents the directional dependence of the slowness $s(\vec{n}) = 1/v(\vec{n})$. It is also known as the refraction or index surface, and apart from a factor of scale is identical to the surface of constant frequency ω or phonon energy $\hbar\omega$ in $\vec{k}$ space. This surface is of great importance in treating reflection and refraction processes at boundaries and is a valuable aid in unravelling the complexities of the ray surface. It is also a surface of three sheets and possesses the same degeneracies as the velocity surface. Multiplying Eq. (1) by s^6 reveals that the equation for this surface is of degree 6 in the components of $\vec{s} = s\vec{n}$. Figure 1 shows a number of sections of the slowness surfaces of Ge and CsCl. The transverse sheets may be observed to become degenerate in the $\langle 100 \rangle$ and $\langle 111 \rangle$ directions and both possess regions of positive and of negative curvature. The longitudinal sheet by contrast is isolated and entirely convex.

The ray or wave surface is defined as the envelope of plane fronts with respect to the velocity surface.[19,20] It follows from this definition that a ray vector $\vec{V}$, and the wave normal $\vec{n}$ that it is associated with, are related by

$$\vec{V} \cdot \vec{n} = v(\vec{n}). \tag{3}$$

The ray and normal are not required to be paral-

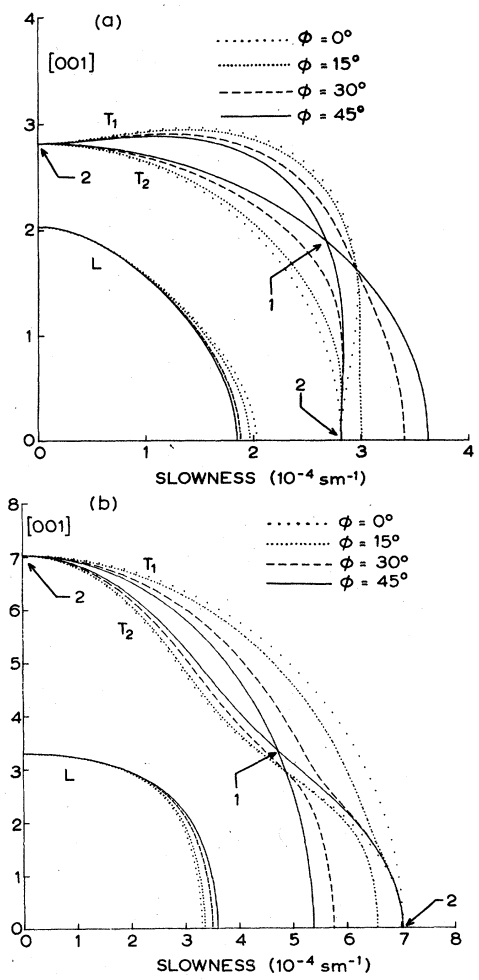

FIG. 1. (a) Polar sections of the slowness surface of Ge showing the variations of $s = 1/v$ with θ for four values of ϕ. The two transverse sheets meet at the conical point (marked 1) in the [111] direction, and make flat contact in the [001] and [100] directions (marked 2). (b) Similar sections for the slowness surface of CsCl.

lel. In fact even in moderately anisotropic crystals the directions of these two vectors can differ quite significantly. On multiplying Eq. (3) by $s = 1/v$ one obtains

$$\vec{V} \cdot \vec{s} = 1 , \tag{4}$$

which shows that the ray and slowness surfaces are polar reciprocals of each other. According to the principle of duality therefore, the degree of the ray surface is equal to the class of the slowness surface, and this places an upper limit of $6(6-1)^2 = 150$ on the degree of the wave surface. The existence of the eight conical points and six smooth contacts reduces this number to $150 - 8(2) - 6(6) = 98$, but this is still so large that the analysis required for deriving and interpreting the equation of the ray surface would not, at present, appear to be a practical proposition.[21] One may conclude, nevertheless, that the complexity of the ray surface, while possibly severe, will be limited to the extent that any straight line can at most meet the surface at 98 points.

There are fortunately other means of calculating the ray surface. One which proves to be convenient in practice is based on the fact that in the absence of dispersion and attenuation the ray and group-velocity vectors coincide, so that $\vec{V}$ may be obtained from the equation[22]

$$\vec{V} = \nabla_{\vec{k}} \omega(\vec{k}) , \tag{5}$$

where $\omega(\vec{k})$ is the frequency which is given by

$$\omega(\vec{k}) = kv(\vec{n}) . \tag{6}$$

It follows from these two equations that[17]

$$\vec{V} = \nabla_{\vec{n}} v(\vec{n}) , \quad V_\alpha = \frac{\partial v}{\partial n_\alpha} , \tag{7}$$

which may be regarded as parametric equations for the ray surface. Methods for evaluating the partial derivatives in Eq. (7) are described in Ref. 18. The ray surface is then simply the locus of points representing the $\vec{V}$'s for all $\vec{n}$.

In the actual computation of the ray surface it is sufficient to take a large but finite number of $\vec{n}$'s distributed uniformly over the unit sphere. The resulting $\vec{V}$'s allow one to visualize the ray surface. In addition, the density with which these $\vec{V}$'s are clustered in various directions provides one with a phonon-enhancement map for the ballistic phonon flux emanating from a localized heat source. One method of displaying the results of such calculations is used in Figs. 4, 6, 11, and 13, which are phonon-enhancement maps for diamond and CsCl. Each point in these diagrams represents the direction of a $\vec{V}(\vec{n})$. Caustics are clearly visible as lines of accumulation of these mode points.

The polar sections of the ray surface of Ge shown in Fig. 3 have been prepared in a similar way, by selecting from a large set of calculated $\vec{V}$'s only those which lie within 0.5° of the particular polar plane. Sectioned folding edges of the ray surface show up clearly as cusps where the mode points accumulate.

A. General considerations concerning the slowness and ray surfaces

With the exception of the eight conical points, each point $\vec{s}(\vec{n})$ on the slowness surface has a unique point $\vec{V}(\vec{n})$ corresponding to it on the ray surface. The ray vectors for the $\vec{n}$'s in the immediate vicinity of any of the conical points on the other hand generate a right circular cone about the particular ⟨111⟩ axis. This effect is known as internal conical refraction.[19] The cone intersects the ray surface on the circle of conical refraction. Points on the ray surface immediately to one side of the circle belong to the T_1 branch while those on the other side belong to the T_2 branch. The two sections of the ray surface match up smoothly on this circle. Under certain conditions a folding edge will touch the circle at six points. Each time it does so the locations of the T_1 and T_2 sections with respect to the circle are reversed. This effect is discussed in more detail in Sec. III.

It follows from Eq. (7) that the group velocity $\vec{V}(\vec{n})$ is perpendicular to the slowness surface at the point $\vec{s}(\vec{n})$. If a small cluster of points on the slowness surface, representing the wave normals for a group of phonons, is considered, then the curvature of the slowness surface is of crucial importance in determining the angular size of the image cluster on the ray surface, and hence the extent to which the phonons are focused.[9] The enhancement of phonon flux by this focusing is measured by the factor[6]

$$A = \frac{\delta\Omega_s}{\delta\Omega_V} , \tag{8}$$

where $\delta\Omega_s$ and $\delta\Omega_V$ are the solid angles subtended by the two clusters in $\vec{s}$ and $\vec{V}$ space, respectively. It is readily shown from this definition of A that

$$A^{-1} = |s^3 V K| , \tag{9}$$

where K is the Gaussian curvature of the slowness surface. At the conical points K diverges and hence the phonon intensity is infinitesimally small on the circles of conical refraction. The other extreme is where K is zero. This gives rise to a caustic on which the phonon intensity is infinite.

The Gaussian curvature is related to the two principal curvatures L_1 and L_2 by

$$K = L_1 L_2 . \tag{10}$$

Since L_1 and L_2 can be positive or negative, the same applies to K. Away from points of degeneracy L_1 and L_2 are continuous functions of $\vec{n}$ and hence the slowness surface can be partitioned into[11] convex regions where L_1 and L_2 are both positive, saddle regions where either L_1 or L_2 is negative, and concave regions where both L_1 and L_2 are negative. These regions are separated by boundary contours, known as parabolic lines, on which $K=0$. The convex and concave regions come into contact only at a discrete set of points, if at all.

The parabolic lines are associated with the folding edges of the ray surface[2] and with caustics in the phonon intensity. For the most part these caustics correspond to the elementary fold catastrophe.[14,23] A number of other types of caustic, however, also occur. Points on the parabolic line where the direction of the vanishing principal curvature is parallel to that line give rise to cusp catastrophe's.[23] A parabolic line will meet a symmetry plane at right angles (except at degeneracy points) and there the two principal curvatures necessarily lie parallel and perpendicular to that plane and consequently also to the line. It is not wholly unexpected therefore to find that for cubic symmetry the majority of cusps are located on symmetry planes. The occurrence of the butterfly and hyperbolic umbilic catastrophes will be described in the next section.

B. Elastic constants and ranges of anisotropy

The shapes of the three characteristic acoustic surfaces of a crystal depend only on the ratios of its elastic constants. The actual magnitudes of the C_{ij}'s and the density of the material merely affect the scale. In cubic symmetry there are three elastic constants, and these are required to satisfy the thermodynamic constraints[24] $C_{44}>0$, $C_{11}>|C_{12}|$, and $C_{11}+2C_{12}>0$.

On a plot of $a=C_{11}/C_{44}$ versus $b=C_{12}/C_{44}$, as shown in Fig. 2, this means a crystal must be located between the two lines $a=-2b$ and $a=b$ in order to be stable. A crystal lying to the left of the first line will have a negative bulk modulus while one situated to the right of the second would have a negative shear modulus in certain orientations.

This wedge-shaped area of stability may be subdivided into a number of zones which are distinguished by the presence or absence of various features in the acoustic surfaces. To start with, below the line $a=1$ where $C_{11}<C_{44}$, the transverse phase velocities exceed the longitudinal velocity in the $\langle 100\rangle$ directions. Similarly, to the left of the line $b=-1$ where $C_{12}<-C_{44}$ the transverse velocities exceed the longitudinal velocity in the $\langle 111\rangle$ directions. It is exceedingly rare to find crystals where the longitudinal mode does not have the largest velocity,[25] and so we will confine attention in what follows to the remaining area. This area is bisected by the line $a=b+2$, which corresponds to the condition for elastic isotropy: $\Delta=C_{11}-C_{12}-2C_{44}=0$. In this isotropic limit the three sheets of the acoustic surfaces are spheres, and the two transverse sheets coincide. These surfaces become progressively more distorted the further a crystal lies from this isotropy line.

A number of definite stages can be distinguished in the development of the shape of these surfaces. In Fig. 2(a), which refers to the T_1 branch, these are represented by the lines A, B, C, D, E and F, and in Fig. 2(b), which applies to the T_2 branch, these stages are given by the lines F, G, and H. Each of these lines signals the change in sign of a principal curvature of the slowness surface near either the $\langle 100\rangle$, $\langle 110\rangle$, or $\langle 111\rangle$ directions which is accompanied by the appearance of a new feature in the folding of the ray surface.

The compilation of elastic constants by Hearmon[26] has been used for positioning the substances that are listed in Fig. 2, with one exception: The constants for diamond (C) are due to Grimsditch and Ramdas.[27]

III. THE SLOWNESS AND RAY SURFACES

A. Longitudinal modes (L)

In the elastic constant domain specified in the preceding section, the mode which in any particular direction has the largest phase velocity, and which therefore is associated with the innermost sheet of the slowness surface, is always longitudinal or at least quasilongitudinal in character. This innermost L sheet is completely separated from the other two sheets, and it follows from the fact that the equation for this surface is of degree 6 that this sheet must be entirely convex.[21] As a consequence, the corresponding sheet of the ray surface can possess no folds and must also be entirely convex.

For crystals with $\Delta=C_{11}-C_{12}-2C_{44}$ negative, i.e., those which lie to the right of the isotropy line in Fig. 2, the L sheet of the slowness surface bulges out and is most convex in the $\langle 100\rangle$ directions [see Fig. 1(a)] where v and V have their minimum values, and is least convex in the $\langle 111\rangle$ directions where v and V are at their maxima. Consequently, longitudinal phonon flux is concentrated or focused most strongly in the $\langle 111\rangle$ directions and is least intense in the $\langle 100\rangle$ directions. These various effects are evident in the sections of the ray surface of Ge shown in Fig. 3. The experi-

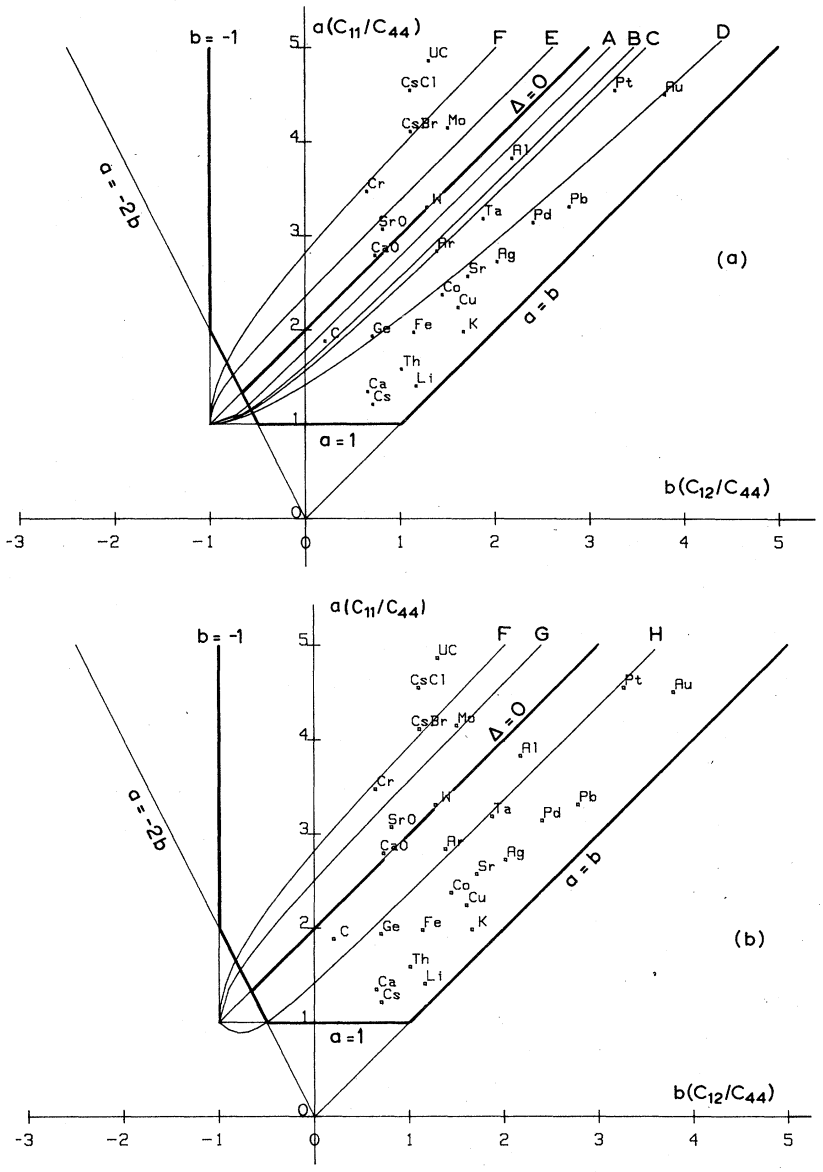

FIG. 2. (a) Conditions on the elastic constants that lead to various singular features in the T_1 sheets of the slowness and ray surfaces discussed in the text. (b) Similar conditions relating to the T_2 sheets.

mental results of Hensel and Dynes[10] confirm that the L modes of Ge are focused in the ⟨111⟩ directions.

For crystals which lie to the left of the isotropy line in Fig. 2 and have Δ positive, the opposite applies. The slowness sheet bulges out in the ⟨111⟩ directions where v and V are at their minima and is flattest in the ⟨100⟩ directions where v and V are at their maxima [see Fig. 1(b)]. The phonon flux is focused towards the ⟨100⟩ directions and away from the ⟨111⟩ directions as can be seen for CsCl in Fig. 4.

B. Slow transverse modes (T_1)

The outermost T_1 sheet of the slowness surface belongs to modes which are quasitransverse in character and which have the smallest of the three phase velocities. It makes contact with the T_2 sheet in the ⟨100⟩ and ⟨111⟩ directions. Except in the isotropy limit this surface possesses both convex and saddle regions, and for certain values of the elastic constants concave regions as well.

On moving from the isotropy condition to the right, i.e., in the direction of increasing b or de-

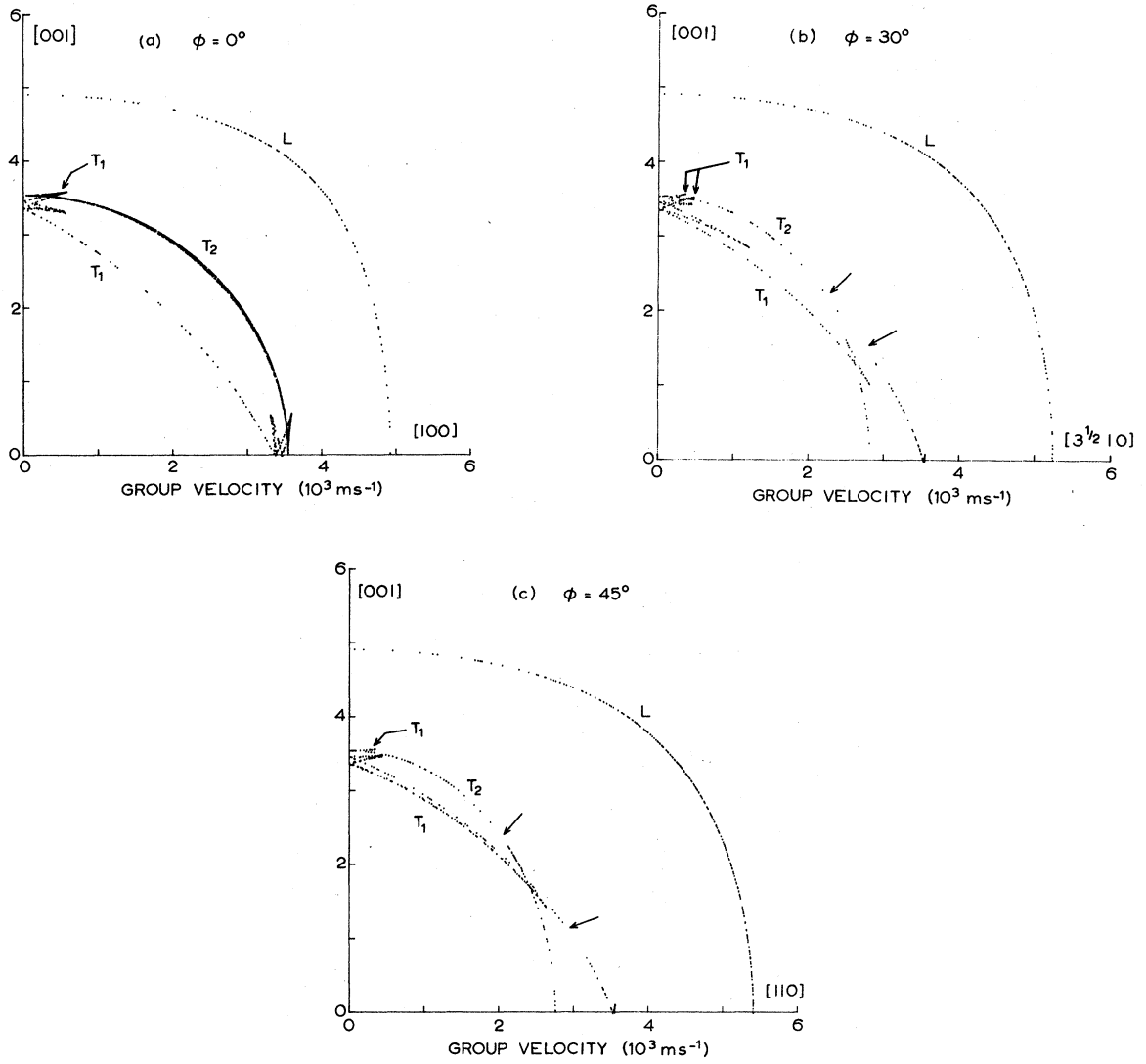

FIG. 3. Polar sections of the ray surface of Ge. A uniform distribution of $\hat{n}$'s on average 0.5° apart has been used to generate a set of ray vectors. Each point represents one of these $\vec{V}$'s which lies within 0.5° of the particular plane. The symmetry plane sections (a) and (c) show more detail than many similarly described diagrams in the literature. This is because they include the effect of $\hat{n}$'s which lie outside the plane but which have $\vec{V}$'s in these planes.

creasing a, the T_1 sheet becomes distorted from spherical. This is most noticeable near the ⟨111⟩ directions where the surface is dimpled inward, with furrows running part of the way towards the neighboring ⟨100⟩ directions. Within these depressions the surface is saddle shaped (i.e., K negative), and each is bounded by a parabolic line separating it from the rest of the surface which is convex (i.e., K positive).

The next important change to come about is the appearance of sets of four furrows radiating outward from each of the ⟨100⟩ directions toward the neighboring ⟨111⟩ directions. This feature requires that the principal curvature transverse to the {110} planes and close to the ⟨100⟩ directions should be negative. This curvature changes sign when

$$2(a-1)(b+1) + (a-b-2)(a+2b+1)(2a+b-1) = 0, \qquad (11)$$

which is represented by line A in Fig. 2. The proof of this and some subsequent results is given in the Appendix.

Figure 5(a) shows the regions of different curvature in the proximity of the irreducible sector of

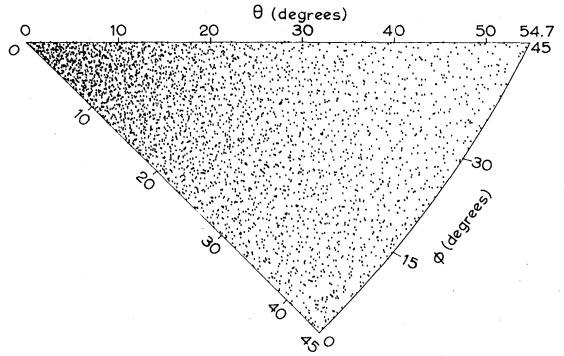

FIG. 4. Phonon-enhancement map for the L mode of CsCl. The mode points correspond to the directions of ray vectors which are associated with $\vec{n}$'s distributed uniformly with an average separation of 0.5°. The map is restricted to the irreducible sector lying between the [001], [101], and [111] directions, and covers 1/48th of the unit sphere.

the unit sphere lying between the [001], [101], and [111] directions. Those marked +− have one principal curvature positive and one negative, and are separated from the ++ regions in which both principal curvatures are positive by parabolic lines (the solid lines). The double-headed arrows at various points on these lines denote the direction of the principal curvature which is zero. The corresponding portion of the ray surface is shown in Fig. 5(b). Folding edges of this surface are represented by solid lines and the dashed line denotes the circle of conical refraction on which the T_1 and T_2 sheets meet. The complete T_1 sheet may be conveniently visualized as consisting of the following three pieces replicated 48 times in accordance with the symmetry operations of the cubic point group:

(*a*) This piece is bounded by the line passing through the points 0′1′2′3′4′6′0′ and is the image of the region 0123460 of the slowness surface.

(*b*) Bounded by 0′1′2′0′ and is the image of the region 0120.

(*c*) Bounded by 4′5′5″3′4′ and is the image of the region 4534. The point 5 has one-sixth of the circle of conical refraction between 5′ and 5″ as its image. Pieces (*a*) and (*b*) are joined along the folding edge 0′1′2′, and (*a*) and (*c*) are joined along the folding edge 3′4′. The cusps at 2′, 3′, and 4′ occur as a result of the vanishing principal curvature at 2, 3, and 4 being parallel to the parabolic line. The fold lines in Fig. 5(b) can also be taken to represent the position of caustics in the phonon intensity. Thus the fold and cusp elementary catastrophes are featured as well as the structurally unstable situation in the [001] direction where eight fold lines converge to a point.

As the anisotropy is increased further, points 2 and 3 approach each other and meet, giving rise to a continuous furrow running between the [111] and [001] directions. As a result cusps 2′ and 3′ of the ray surface annihilate and pieces (*b*) and (*c*) join up into a single piece. Two crystals that exhibit the type of surface that now results are diamond and aluminium. Figure 6 shows the phonon-enhancement map for the former.

As the anisotropy is increased further the furrows broaden out near the [001] direction and then

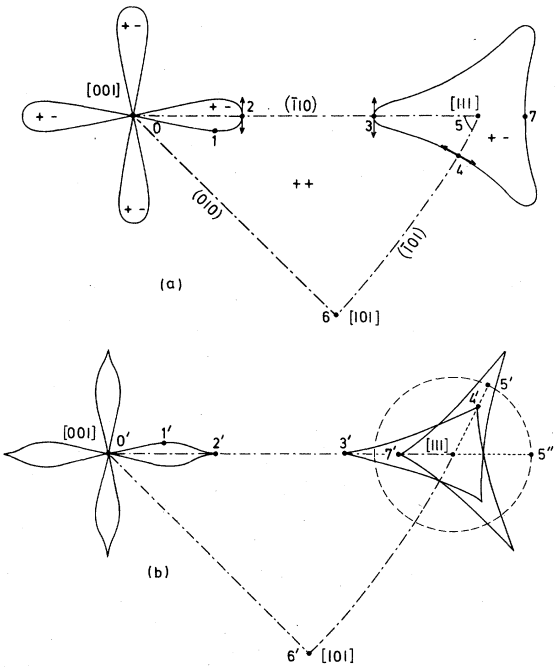

FIG. 5. (a) Regions of different curvature for the T_1 sheet of the slowness surface when the anisotropy lies just beyond A. (b) Disposition of folds in the ray surface, which correspond to caustics in the phonon-enhancement map.

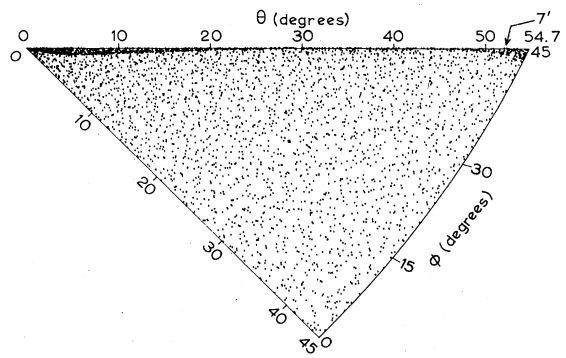

FIG. 6. Phonon-enhancement map for the T_1 mode of diamond. The cusps 2′ and 3′ in Fig. 5(b) have just met. The cusp 7′ can only just be discerned.

merge so that all around this direction the slowness surface is saddle shaped. This occurs as the in-plane curvature in the {100} planes near the ⟨100⟩ directions changes sign, i.e., when

$$a(a-1)-(b+1)^2=0\,, \tag{12}$$

which is represented by line B in Fig. 2(a). The folds in the ray surface, instead of terminating in the [001] direction, now sweep around this point in the manner shown in Fig. 7(b) (disregarding the presence of the "Maltese-cross"-shaped figure for the moment).

The next development with increasing anisotropy is the appearance of the concave regions marked – – in Fig. 7(a). These accompany the change in sign of the in-plane curvature in the {110} planes near the ⟨100⟩ directions. This takes place when

$$a^2+(a-1)(b+1)-2(b+1)^2-1=0\,, \tag{13}$$

which is represented by line C in Fig. 2(a).

The "Maltese-cross"-shaped system of folds shown in Fig. 7(b) that has appeared in the wave surface is the image of the parabolic line around the – – regions of the slowness surface. The cusps correspond to points such as 1 on this contour. A new piece (d) bounded by 0′1′2′0′ and which is the image of 0120 now exists. It is joined to piece (bc) along the fold edges 0′1′ and 1′2′ and piece (bc) now partly overlaps itself. Examples of crystals that possess this type of ray surface are Ge, Si, Ta, and Pt. The three-chain dotted lines in Fig. 7(b) show the location of the $\phi = 0°$, $\phi = 30°$, and $\phi = 45°$ sections of the ray surface of Ge that are depicted in Fig. 3. The folding edges show up as cusps in these sections. In the {100} planes pieces (bc) and (d) lie extremely close together and are in fact not resolved in Fig. 3(a). The points where the T_1 and T_2 sheets of the ray surface meet on the circle of conical refraction are marked by arrows in Fig. 3. These diagrams indicate how many components a heat pulse will split up into on propagating in various directions, and also how these components will be spaced out and what their relative intensities will be.[28] Experimental limitations will, of course, ultimately determine the extent to which the individual components can be resolved. Concerning Ge it may be noted that there are three T_1 components that propagate in the [001] direction. For the fastest component, $\vec{n}$ is parallel to [001], the intermediate one consists of phonons of four equivalent $\vec{n}$'s lying in the (110) and ($\bar{1}$10) planes to either side of the [001] direction, and the slowest consists of phonons with four equivalent $\vec{n}$'s lying in the (100) and (010) planes near to [001]. It is also interesting to note that a sizable portion of the T_1 sheet (in the vicinity of the ⟨100⟩ directions) lies outside the T_2 sheet, and so there are many slow transverse modes which "travel faster" than fast transverse modes which are propagating in the same direction.

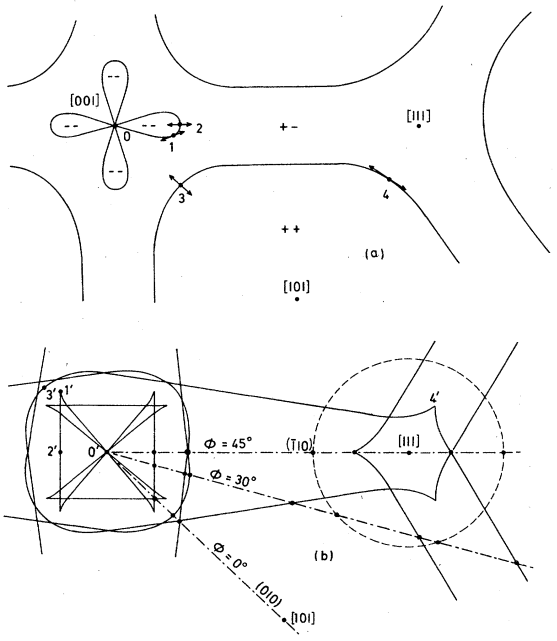

FIG. 7. (a) Regions of different curvature for the T_1 sheet of the slowness surface when the anisotropy lies between C and D. (b) Disposition of folds in the ray surface. Chain dotted lines denote location of sections of the ray surface of Ge shown in Fig. 3.

The Maltese cross and surrounding system of caustics have previously been shown by Northrop and Wolfe[11] to fit very accurately their experimental results on ballistic phonons in Ge. The peaks near the [001] and [111] directions that Hensel and Dynes[10] observe in their phonon imaging of Ge can also readily be interpreted in terms of the caustics in Fig. 7(b). A calculated phonon-enhancement map for Ge has been discussed by this author.[18]

As the anisotropy increases further, the – – lobes on the slowness surface expand and then merge to form a continuous region around the [001] direction where the surface is concave [see Fig. 8(a)]. This occurs as the principal curvature transverse to the cube planes near the ⟨100⟩ directions changes sign, which takes place when

$$(a-1)(a+b)+(a-b-2)(b+1)^2=0\,. \tag{14}$$

This equation is represented by line D in Fig. 2(a). Simultaneously the limbs of the Maltese cross break away from the [001] axis and terminate in four cusps in the (100) and (010) planes. Each limb, as can be seen in Fig. 8(b), now consists of

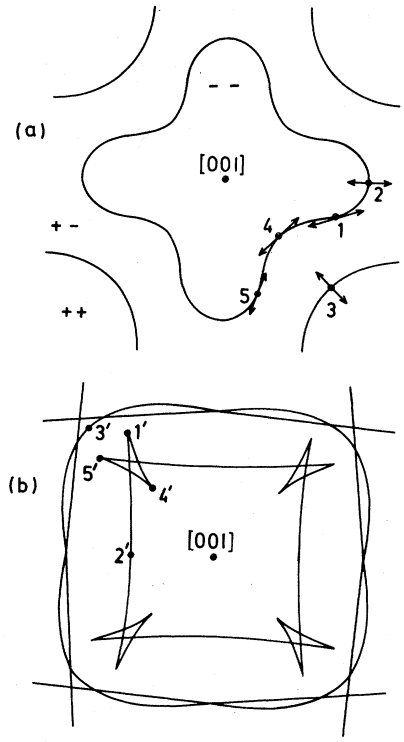

FIG. 8. (a) Curvature of the slowness surface near [001] when the anisotropy lies beyond D. (b) Shows the butterfly catastrophe formed by cusps 1′ and 4′ and 5′.

three cusps in the form of the butterfly catastrophe.[29]

Moving now in the direction of decreasing a, points 1 and 5 merge with point 4 causing the three cusps 1′, 5′, and 4′ to coalesce into a single cusp, shown as 4′ in Fig. 9(a). This cusp then approaches the neighboring fold line and meets it to give rise to the hyperbolic umbilic catastrophe[23] shown in Fig. 9(b). The ray surface which has been calculated for Cu by Miller and Musgrave conforms to this special case.[1]

The unfolding of this hyperbolic umbilic results again, as shown in Fig. 9(c) in a cusp and a smooth fold line, but with the latter now being the remnant of the cross. The highly anisotropic metals Cs, Li, and Ca are examples of crystals that display this last type of feature. The transformations depicted in Fig. 9 occur as points 4 and 3 in Fig. 8(a) approach, meet, and then recede from each other, but with the directions of the vanishing principal curvatures now interchanged.

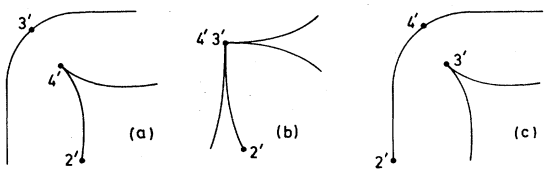

FIG. 9. Hyperbolic umbilic catastrophe formed as the cusp 4′ approaches the neighboring fold line at 3′.

On the other side of the isotropy line, i.e., in the direction of increasing a or decreasing b, the evolution of the T_1 sheet is initially similar to that described above. To start with, as the anisotropy is increased the dimples appear on the slowness surface in the ⟨111⟩ directions. Subsequently, furrows appear around the ⟨100⟩ directions when

$$2a^2 - 3a + ab - 3b^2 - 9b - 4 = 0\,, \tag{15}$$

which is represented by line E in Fig. 2(a), and these furrows radiate outwards to meet with the depressed regions around the dimples.

No further significant changes occur in the vicinity of the ⟨100⟩ directions, but beyond line F in Fig. 2(a), which is given by

$$6(a-b+1)^2(b+1) - 3(a-b-2)^2(b+1) - (a-b+1)(a-b-2)(8a+13b+5) = 0\,, \tag{16}$$

there are three concave regions that meet each conical point [see Fig. 10(a)]. The in-plane curvature in the $(\bar{1}10)$ plane to one side of the [111] direction is now negative as can be seen in the $\phi = 45°$ section of CsCl shown in Fig. 1(b). The parabolic line around these three regions results

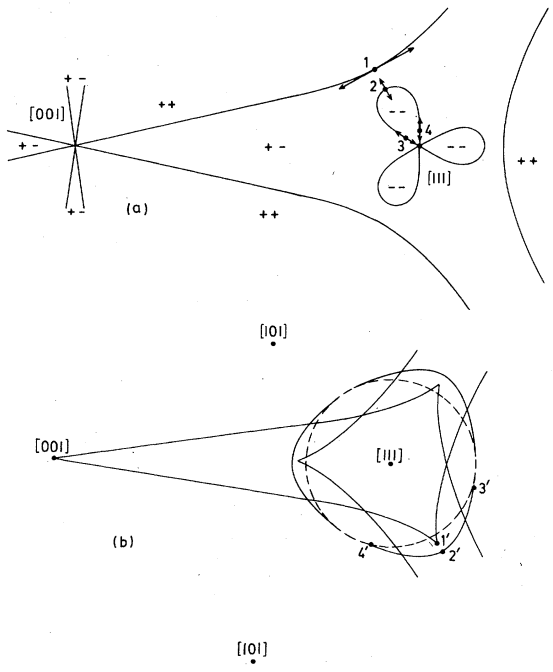

FIG. 10. (a) Curvature of the T_1 sheet of the slowness surface beyond F. (b) Disposition of folds in the ray surface.

in three fold lines in the ray surface which bulge outwards from the circle of conical refraction [see Fig. 10(b)]. These do not end in cusps, as might be expected in view of the direction of the vanishing principal curvatures at 3 and 4, but meet the circle tangentially. The missing portions of these fold lines, needed for continuity, are to be found in the T_2 sheet. Between points such as 3′ and 4′ the T_1 sheet extends beyond the circle of conical refraction, is folded across the line 3′2′4′, and then approaches the circle from outside. Here it joins up smoothly with the T_2 sheet which between 3′ and 4′ approaches the circle from the inside.

The above situation gives rise to a remarkable effect in the phonon intensity. The six points where the fold line touches the circle of conical refraction lie on a caustic, where the enhancement is infinite as well as on the circle of conical refraction where the enhancement is zero, so that the phonon enhancement cannot be uniquely defined at these points. This is related to the fact that the curvature of the slowness surface at the conical point does not have a unique value. It tends to $-\infty$, 0, or $+\infty$ depending on the direction of approach. In the phonon-enhancement map for CsCl shown in Fig. 11 this caustic is only faintly visible compared with the other much more prominent caustic that is present. One conclusion that may be drawn from this is that while the analysis in terms of caustics is important in gaining a deeper understanding of the main features in phonon-imaging patterns,[11] the calculation of the detailed phonon-enhancement map is necessary for a complete interpretation of experimental results.

C. Fast transverse modes (T_2)

The third or T_2 sheet of the slowness surface lies between the other two, and belongs to the fast quasitransverse modes. It is formed into conical shaped peaks in the ⟨111⟩ directions, and there it meets with the inward projecting dimples of the T_1 sheet. It also makes smooth contact with the T_1 sheet in the ⟨100⟩ directions. It is entirely convex when the anisotropy is small, and the corresponding sheet of the ray surface therefore possesses no folds.

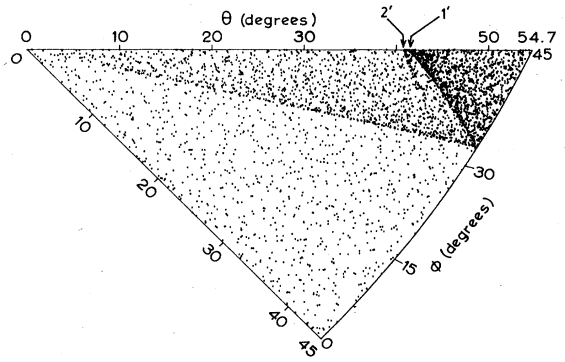

FIG. 11. Phonon-enhancement map for the T_1 mode of CsCl. The caustic that meets the circle of conical refraction is much fainter than the other caustic, and almost forms a hyperbolic umbilic catastrophe with it.

Furrows, running between adjacent ⟨100⟩ directions, appear in the T_2 sheet of the slowness surface when the anisotropy reaches line H in Fig. 2(b). This line is given by the equation

$$a^2+ab-2(b+1)^2=0\,. \tag{17}$$

The curvature transverse to the {100} planes is now negative.

The ray surface, under these circumstances, is folded on either side of the cube planes, with two fole lines running between each pair of adjacent ⟨100⟩ directions. The T_2 sheet approaches the circle of conical refraction from outside and meets up there with the T_1 sheet. Miller and Musgrave[1] have described this case in more detail. The caustics in the phonon intensity, associated with these folding edges, show up prominently in experimental results on Ge.[10,11] The folding and the effect of the close proximity of the caustics to the (010) plane are both apparent in Fig. 3.

To the left of the isotropy line the T_2 sheet of the slowness surface remains convex until

$$(2a+b-1)(a-b-2)-2(b+1)=0\,, \tag{18}$$

which is represented by line G in Fig. 2(b). At this point, in the ⟨110⟩ directions, the curvature in the cube planes changes sign. Small +− regions develop around the ⟨110⟩ direction such as the one bounded by the chain dotted parabolic line in Fig. 12(a). The ray surface, as a consequence, becomes folded in the way shown by the chain dotted line in Fig. 12(b).

As the anisotropy is increased further, the +− regions of the slowness surface expand to eventually surround the ⟨111⟩ directions, but in the process leaving small ++ islands at the conical points as shown by the solid lines in Fig. 12(a). This process is completed as the anisotropy goes through line F which is given by Eq. (16). The resulting system of folds in the ray surface is shown by the solid lines in Fig. 12(b). Attached to the circle of conical refraction there are now fold lines such as 7′5′6′ which meet the circle tangentially and then penetrate through to the T_1 sheet as described earlier. Between points such as 6′ and 8′, the T_2 sheet approaches the circle of conical refraction from the inside. Between points such as 7′ and 6′ it crosses the circle to the outside, is folded along 7′5′6′ and then approaches

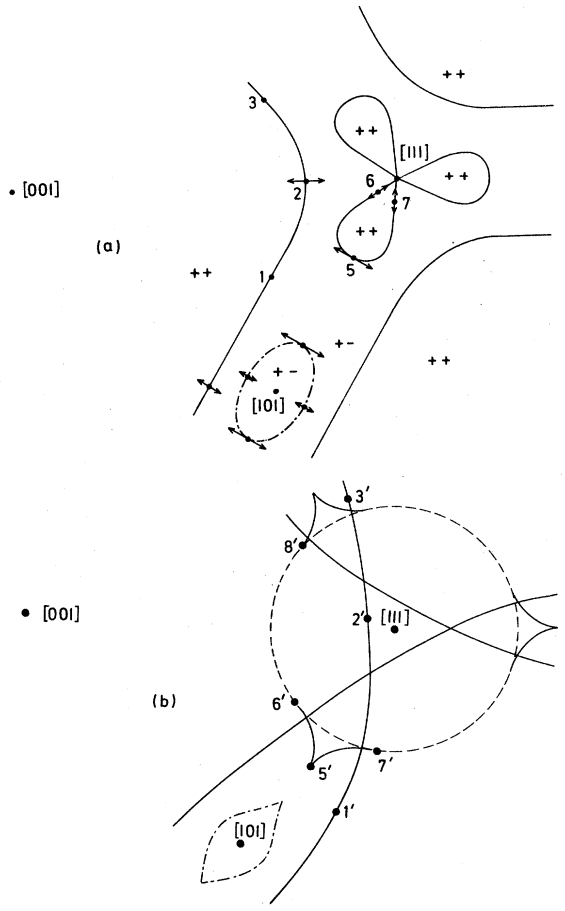

FIG. 12. (a) Curvature of the T_2 sheet of the slowness surface beyond G (chain dotted line) and beyond F (solid line). (b) Disposition of folds in the ray surface.

the circle from the outside. Figure 13 shows the phonon-enhancement map for the T_2 mode of CsCl. As in the case of the T_1 mode, the caustic that meets the circle is relatively faint and would probably be difficult to detect experimentally.

IV. SUMMARY AND CONCLUSIONS

The acoustic slowness and ray surfaces of cubic crystals have been shown to exhibit considerable variation in shape depending on the degree of elastic anisotropy. The major emphasis has been on determining the different ways in which the ray surface can be folded and thus what systems of caustics can occur in the phonon-intensity map. As long as $C_{11} > C_{44}$ and $C_{12} > -C_{44}$ the longitudinal sheet of the ray surface does not possess any folds and is entirely convex. The T_1 sheet displays numerous systems of folds depending on the degree of anisotropy, while the T_2 sheet shows slightly less variation.

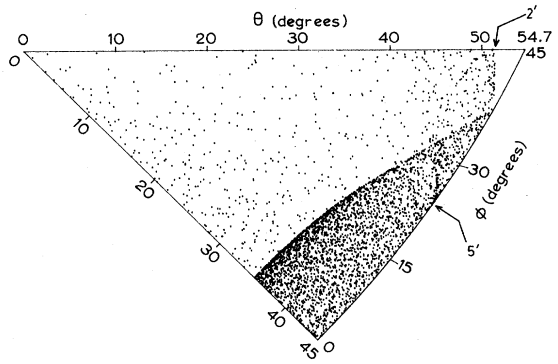

FIG. 13. Phonon-enhancement map for the T_2 mode of CsCl. As with the T_1 mode, the fold caustic that meets the circle of conical refraction is relatively faint.

Away from the ⟨100⟩ and ⟨111⟩ directions the curvature of the slowness surface is uniquely defined at every point. The caustics that occur as a result of this curvature being zero are of the structurally stable type, with the fold, cusp, hyperbolic umbilic, and butterfly catastrophes being featured for various values of the elastic constants. Some remarkable forms of structural instability result from the degeneracy of the T modes in the ⟨100⟩ and ⟨111⟩ directions.

From examples given, it is clear that phonon-intensity caustics can vary considerably in prominence. In interpreting phonon-imaging results therefore, it is important to calculate the full phonon-enhancement map as well as the locations of the caustics.

APPENDIX

We outline here a method for deriving Eqs. (11)–(18). Let Θ and Φ denote the polar and azimuthal angles, respectively, of the normal to the slowness surface in the direction (θ, ϕ). Then

$$\tan\Theta = (V_x^2 + V_y^2)^{1/2}/V_z , \tag{A1}$$

and

$$\tan\Phi = V_y/V_x , \tag{A2}$$

where V_x, V_y, and V_z are the Cartesian components of the group velocity which is also normal to this surface. These components may be expressed in terms of the phase velocity v and its derivatives by[18]

$$V_x = v\sin\theta\cos\phi + \frac{\partial v}{\partial\theta}\cos\theta\cos\phi - \frac{\partial v}{\partial\phi}\frac{\sin\phi}{\sin\theta} , \tag{A3}$$

$$V_y = v\sin\theta\sin\phi + \frac{\partial v}{\partial\theta}\cos\theta\sin\phi + \frac{\partial v}{\partial\phi}\frac{\cos\phi}{\sin\theta} , \tag{A4}$$

and

$$V_z = v\cos\theta - \frac{\partial v}{\partial \theta}\sin\theta . \tag{A5}$$

In a symmetry plane the directions of the two principal curvatures of the slowness surface lie in, and perpendicular to, this plane. In particular, if this plane contains the z axis then the two curvatures are proportional, respectively, to

$$\frac{\partial \Theta}{\partial \theta} \quad \text{and} \quad \frac{\sin\Theta}{\sin\theta}\frac{\partial \Phi}{\partial \phi} .$$

Near the [001] direction the two transverse velocities are given to second order in θ by[30]

$$\left(\frac{\rho}{C_{44}}\right)^{1/2} v = 1 + \frac{\Delta_1 \theta^2}{4C_{44}}\{\Delta_2 \pm [\Delta_2^2 - \sin^2 2\phi(2\Delta_2 - 1)]^{1/2}\}, \tag{A6}$$

where

$$\Delta_1 = C_{11} - C_{12} - 2C_{44} ,$$

and

$$\Delta_2 = \Delta_1/(C_{44} - C_{11}) + 2 .$$

With the use of this velocity expression and by setting

$$\left.\frac{\partial \Theta}{\partial \theta}\right|_{\phi = 0, \pi/4} = 0 , \tag{A7}$$

one obtains Eqs. (12) and (13), while by setting

$$\left.\frac{\partial \Phi}{\partial \phi}\right|_{\phi = 0, \pi/4} = 0 , \tag{A8}$$

one obtains Eqs. (11), (14), (15), and (17). Similarly by using the well-known velocity expressions that apply in the (010) and ($\bar{1}$10) planes for cubic crystals[19,22] and by setting

$$\left.\frac{\partial \Theta}{\partial \theta}\right|_{\phi = \pi/4,\, \theta = \arccos(1/3^{1/2})} = 0 , \tag{A9}$$

and

$$\left.\frac{\partial \Theta}{\partial \theta}\right|_{\phi = 0,\, \theta = \pi/4} = 0 , \tag{A10}$$

one obtains Eqs. (16) and (18), respectively. Equations (12), (13), (17), and (18) have previously[3-6] been mentioned in the literature, but Eqs. (11), (14), (15), and (16) are presented here for the first time.

[1] G. F. Miller and M. J. P. Musgrave, Proc. R. Soc. London Ser. A 236, 352 (1956).
[2] F. Rösch and O. Weis, Z. Phys. B 25, 101 (1976); 25, 115 (1976).
[3] M. J. P. Musgrave, Proc. Cambridge Philos. Soc. 53, 897 (1957).
[4] M. J. P. Musgrave, J. Elastic. 9, 105 (1979).
[5] S. R. Prabhakaran Nayar and K. S. Viswanathan, Can. J. Phys. 50, 1903 (1972).
[6] H. J. Maris, J. Acoust. Soc. Am. 50, 812 (1971).
[7] J. Philip and K. S. Viswanathan, Phys. Rev. B 17, 4969 (1978).
[8] C. G. Winternheimer and A. K. McCurdy, Phys. Rev. B 18, 6576 (1978).
[9] B. Taylor, H. J. Maris, and C. Elbaum, Phys. Rev. B 3, 1462 (1971).
[10] J. C. Hensel and R. C. Dynes, Phys. Rev. Lett. 43, 1033 (1979).
[11] G. A. Northrop and J. P. Wolfe, Phys. Rev. Lett. 43, 1424 (1979).
[12] W. Eisenmenger, in *Phonon Scattering in Condensed Matter*, edited by H. J. Maris (Plenum, New York, 1980), pp. 303–308.
[13] A. K. McCurdy, H. J. Maris, and C. Elbaum, Phys. Rev. B 2, 4077 (1970).
[14] P. Taborek and D. L. Goodstein, Phys. Rev. B 22, 1550 (1980).
[15] M. Greenstein and J. P. Wolfe, Phys. Rev. Lett. 41, 715 (1978); R. S. Markiewicz, M. Greenstein, and J. P. Wolfe, Solid State Commun. 35, 339 (1980).
[16] P. Taborek and D. Goodstein, J. Phys. C 12, 4737 (1979).
[17] F. I. Fedorov, *Theory of Elastic Waves in Crystals* (Plenum, New York, 1968).
[18] A. G. Every, Phys. Rev. B 22, 1746 (1980).
[19] M. J. P. Musgrave, *Crystal Acoustics* (Holden-Day, San Francisco, 1970).
[20] M. J. P. Musgrave, Proc. R. Soc. London Ser. A 226, 339 (1954).
[21] G. F. D. Duff, Philos. Trans. R. Soc. London 252, 249 (1960).
[22] B. A. Auld, *Acoustic Fields and Waves in Solids* (Wiley, New York, 1973), Vol. 1.
[23] M. V. Berry, Adv. Phys. 25, 1 (1976).
[24] J. F. Nye, *Physical Properties of Crystals* (Oxford University Press, London, 1957).
[25] The only clear-cut case to the author's knowledge is that of the intermediate valence compound $Tm_{0.99}Se$. See H. Boppart, A. Treindl, and P. Wachter, Solid State Commun. 35, 483 (1980). A marginal situation in which $C_{11} \simeq C_{12} \simeq C_{44}$ is provided by the martensitic transformation in fcc manganese alloys. See M. Sato, R. D. Lowde, G. A. Saunders, and M. M. Hargreave, Proc. R. Soc. London Ser. A 374, 115 (1981).
[26] R. F. S. Hearmon, in *Landolt-Börnstein: Numerical Data and Functional Relationships in Science and Technology*, New Series, edited by K.-H. Hellwege (Springer, Berlin, 1979), Group III, Vol. II, pp. 1–244.
[27] M. H. Grimsditch and A. K. Ramdas, Phys. Rev. B 11, 3139 (1975).
[28] In comparing heat pulse *intensities* the density of mode points should be multiplied by a factor $1/v^3$ to take account of the heat capacity of the modes.
[29] E. C. Zeeman, *Catastrophe Theory* (Addison-Wesley, Reading, Mass., 1977).
[30] P. C. Waterman, Phys. Rev. 113, 1240 (1959).